Applied Physics Letters ARTICLE pubs.aip.org/aip/apl

Characteristic voltages and times from capacitance–voltage analysis of quantum dot light-emitting diodes

Cite as: Appl. Phys. Lett. **124**, 263503 (2024); doi: 10.1063/5.0221019
Submitted: 29 May 2024 · Accepted: 17 June 2024 ·
Published Online: 27 June 2024

Xiangwei Qu,[1,2] Jingrui Ma,[1,2] Kai Wang,[1,2] and Xiao Wei Sun[1,2,a)]

AFFILIATIONS

[1]Institute of Nanoscience and Applications, and Department of Electrical and Electronic Engineering, Southern University of Science and Technology, Shenzhen 518055, China
[2]Key Laboratory of Energy Conversion and Storage Technologies (Southern University of Science and Technology), Ministry of Education, Guangdong University Key Laboratory for Advanced Quantum Dot Displays and Lighting, and Shenzhen Key Laboratory for Advanced Quantum Dot Displays and Lighting, Southern University of Science and Technology, Shenzhen 518055, China

[a)]Author to whom correspondence should be addressed: sunxw@sustech.edu.cn

ABSTRACT

The characteristic voltages in the capacitance–voltage (C–V) curve of quantum dot light-emitting diodes (QLEDs) are usually linked to the start of charge injection and recombination in a working device. However, it may lead to a misunderstanding of the carrier process in QLEDs. This is because capacitance change only reflects an electrical response of additional carriers induced by a small signal loaded on an applied DC voltage but does not directly correlate with the total free carrier response governed by the working voltage. In this work, we study the frequency-dependent C–V characteristics of a blue QLED, focusing on the characteristic voltages, characteristic times, and their relationships. First of all, we identify that the charge injection point of QLEDs should be extracted by the current density–voltage–luminance characteristics rather than the C–V curve. As for the characteristic voltages obtained from the C–V curve, they are determined by voltage-dependent characteristic times in different time domains. Furthermore, the C–V characteristic is helpful to evaluate charge accumulation or leakage in blue QLED, serving as an accessible analysis tool in the carrier transport process. Our work provides a definite physical meaning of characteristic voltages in the C–V curve and exhibits the usefulness of C–V characteristics for analyzing the charge dynamics of QLED.

Quantum dot light-emitting diode (QLED) is considered a promising candidate for next-generation flat-panel display technology for its narrow linewidth, high performance, and low-cost fabrication process.[1–6] In a working QLED device, the fundamental carrier processes involve charge injection, transport, and trapping, as well as exciton formation and recombination.[4–6] Especially, charge injection balance is a key factor influencing QLED performance, which is determined by the carrier injection and transport processes. Moreover, the sub-bandgap turn-on voltage of QLED is tightly connected with the charge injection process. The charge recombination process is crucial to improve the radiative emission efficiency. Though there are many studies on these fundamental processes, the charge injection mechanism and the exciton dynamics of QLED still remain unclear,[2,4–6] which needs a more in-depth characterization method to understand the underlying physics, ultimately leading to improvements in QLED efficiency and stability.

Impedance spectroscopy is a nondestructive tool to study the electrical parameter and carrier processes of a semiconductor optoelectronic device.[7–9] It is now widely employed to provide valuable insight into charge dynamics in QLED.[10–19] Typically, a Nyquist plot aids in constructing an equivalent circuit model, facilitating the extraction of transport and recombination resistance in a working QLED.[13,14] The Mott−Schottky analysis can yield the built-in voltage of a single-carrier device.[15,16] A capacitance–frequency (C–f) characteristic is commonly utilized to determine defect distribution, serving as a useful tool for exploring the charge trapping process.[17–19] The capacitance–voltage (C–V) characteristic is also appropriate to depict the charge injection and recombination process of QLED since it directly correlates with the space charge changes in a QLED device,[7] i.e., $\Delta Q = C\Delta V$ (ΔQ is the change of space charge amounts, C is the device capacitance, and ΔV is the step of working voltage). Usually,

charge injection and trapping processes contribute to an increase in device capacitance, while charge recombination depletes the free carrier, resulting in a decrease in capacitance. Therefore, the capacitance changes in a C–V curve reflect the electroluminescence process in QLED.

The carrier processes revealed by the C–V characteristic are shown as follows:[20–22] The majority carrier (electron) is first injected into the device at the characteristic voltage that capacitance starts to rise (V_t), and the minority carrier (hole) is injected in sequence at the characteristic voltage of peak capacitance (V_p). Then electrons and holes recombine, depleting the free carrier, thereby leading to the capacitance drop. That is to say, electrons and holes are injected in sequence at different voltages, and QLED turns on after V_p, similar to the case of an organic light-emitting diode.[7–9] This represents the first QLED C–V model. However, recent findings indicate that the QLED device emits at V_t, suggesting that the capacitance rise is accompanied by a bipolar carrier injection, i.e., electrons and holes are simultaneously injected, and QLED turns on after V_t, which constitutes the second QLED C–V model.[23,24] Therefore, the precise physical meaning of these characteristic voltages in a C–V curve remains unclear, which warrants of a more detailed and comprehensive study.

In this work, we study the C–V characteristics of a CdSe-based blue QLED, focusing on the characteristic voltages and characteristic times of the C–V curve and their relationships. We found that the charge injection point of a QLED should be extracted by the current density–voltage–luminance (J–V–L) characteristics rather than a C–V curve. As for the characteristic voltage in the C–V curve, it is determined by the transition time for charge injection and recombination time at the selected working voltage. Additionally, a C–V curve helps to evaluate charge accumulation or leakage in the blue QLED. Our work gives a definite physical meaning to the characteristic voltages and demonstrates the applications of C–V characteristics in understanding the charge dynamics of QLEDs.

Our blue QLED ($\lambda_{EL} = 472$ nm, Fig. S1) is structured as ITO/poly (3,4-ethylenedioxythiophene): polystyrene sulfonate (PEDOT:PSS)/poly(9,9-dioctylfluorene-co-N-(4-(3-methyl propyl)) diphenylamine) (TFB)/QD/ZnMgO/Al, where ITO, PEDOT:PSS, TFB, blue QD, ZnMgO, and Al work as the anode, hole injection layer, hole transport layer (HTL), emission layer, electron transport layer, and cathode, respectively. The patterned ITO glass was treated by UVO for 15 min before film deposition. Subsequently, PEDOT:PSS, TFB, blue QD, and ZnMgO layers were spin-coated on ITO glass layer by layer. After that, the sample was transferred to a vacuum evaporation chamber to deposit a 100 nm Al electrode. Before any electrical test, the blue QLED device was well encapsulated in dry nitrogen. The J–V–L characteristics of blue QLED were measured by a dual-channel Keithley 2614B source measurement unit and a PIN-25D silicon photodiode. The C–V and C–f characteristics of the blue QLED were conducted using the Fluxim Paios measurement system at room temperature within the frequency ranging from 100 Hz to 1 MHz under an applied voltage from 0 to 5 V. The amplitude of the AC signal was configured to 100 mV, ensuring a linear electrical response without significantly affecting the working voltage.[7,12]

Figure 1 displays the J–V–L and C–V characteristics of a blue QLED, and the C–V characteristics of QLED are conducted at a frequency of 1 kHz. We usually analyze the electroluminescence process of blue QLED by correlating these three curves. Under low applied

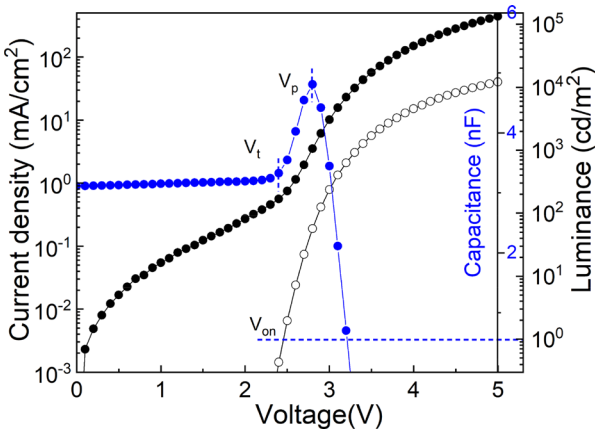

FIG. 1. J–V–L and C–V characteristics of the blue QLED.

bias before device turn-on, the capacitance of the device is contributed by geometrical capacitance (C_g) and remains constant, implying no free carrier injection into the device. Increasing bias to V_t (2.4 V), the capacitance starts to rise, corresponding to the turn-on voltage (V_{on}) at 1 cd/m^2, which is located between 2.4 and 2.5 V in the L–V characteristic. This V_t point signifies the simultaneous occurrence of bipolar carrier injection and exciton recombination, which is consistent with the second QLED C–V model. Upon reaching the bias V_p (2.8 V), there is a significant and abrupt drop in device capacitance, which is attributed to the dominating process of exciton recombination, rapidly depleting free carriers and even resulting in negative capacitance.[10] Therefore, the electroluminescence process including charge injection and recombination can be analyzed using the C–V characteristic. In the J–V curve, the transition voltage between the Ohmic conduction region and trap charge-limited conduction region is 2.5 V, consistent with the turn-on voltage in the L–V characteristic and V_t in the C–V curve. Therefore, these three curves closely correlate with each other, providing a comprehensive depiction of the carrier behavior in blue QLED.

However, when the C–V characteristic of blue QLED is conducted at different frequencies, the characteristic voltages vary with the frequency, indicating frequency-dependent carrier processes in a blue QLED. As shown in Fig. 2(a), the feature of the C–V characteristics is highly dependent on applied frequency. For instance, C_g of blue QLED shows a slight decrease as the frequency increases, while the peak capacitance of the device significantly drops with increasing frequency. In particular, the characteristic voltage shifts in these C–V curves with varied frequency is evident. Specifically, V_t increases from 2.2, 2.3, 2.4 to 2.7 V, and V_p increases from 2.6, 2.7, 2.8 to 2.9 V at the frequencies of 100 Hz, 500 Hz, 1 kHz, and 5 kHz, respectively. At 100 Hz, the charge injection and recombination behavior match more closely to the first QLED C–V model, since V_p is near the turn-on voltage. This implies electron injection at 2.2 V followed by hole injection at 2.6 V. Starting from 2.6 V, electron and hole recombination consumes the carrier, resulting in the capacitance drop of QLED. Conversely, at 1 kHz, the second QLED C–V model is more suitable, where electron and hole are injected into the device simultaneously at 2.4 V, presenting a different carrier transport picture compared to the 100 Hz case. Therefore, the two proposed C–V models 1 and 2 are not appropriate

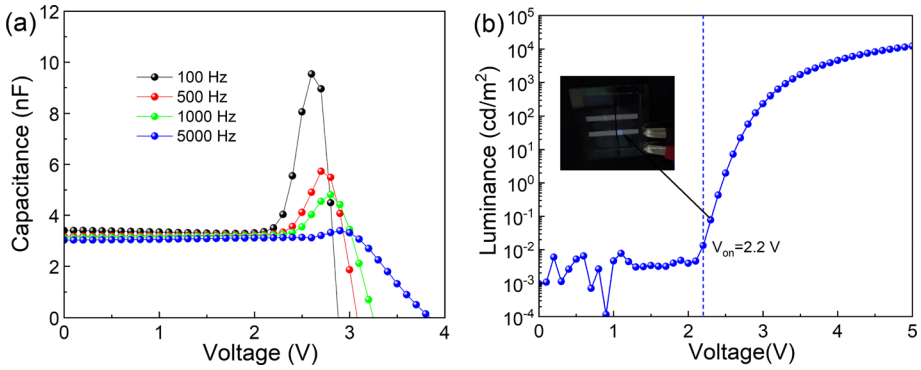

FIG. 2. (a) C–V characteristics of the blue QLED at varied frequencies, and (b) L–V characteristic of the blue QLED, the inset shows the picture of QLED lighting up at 2.3 V.

to depict the charge injection and recombination process, because the applied frequency can potentially lead to a misunderstanding of the physical process and device parameters. Several questions remain to be clarified in our C–V experiment: (i) where is the actual charge injection point in a C–V curve? and (ii) what do V_t and V_p mean in a C–V curve, and what determines them in this context?

In our experiment, we have observed a faint blue emission at 2.2 V ($L = 0.02$ cd/m^2) below the turn-on voltage. The inset in Fig. 2(b) shows a clear emission of the device at 2.3 V, while the photo at 2.2 V lacks clarity (not shown). However, we consider it reasonable to reset V_{on} of blue QLED to be 2.2 V (not between 2.4 and 2.5 V, referring to Fig. 1), as the luminance level at this point is one order of magnitude higher than the background [Fig. 2(b)]. Therefore, we identify that the charge injection point is at the working voltage of 2.2 V. Furthermore, the turn-on voltage should be extracted in the J–V–L curve rather than in the C–V one. This is due to the fact that V_t in the C–V curves is not fixed and highly depends on the applied frequency. Actually, a C–V curve solely presents the electrical response of carriers due to the small signal loaded on the applied DC bias,[7,12] while the charge injection point signifies the case where a large number of free carriers are injected into the device, driven by the applied DC bias. Therefore, it is not appropriate to identify the charge injection point in a C–V curve. Instead, V_t is helpful to determine if the additional carriers generated by the small AC signal are injected into the device. Of course, it requires the DC bias to be equal to or larger than V_{on}, i.e., the charge injection point in a J–V–L curve.

As for the characteristic voltages V_t and V_p, they are determined by the characteristic times, which comprises transition time τ_{tr} for charge injection and recombination time τ_r for electron and hole recombination. First of all, to observe the characteristic voltage V_t and V_p in the C–V curve after V_{on}, it requires that τ_{tr} is smaller than the period of the AC voltage τ_{ac} ($\tau_{ac} = 1/f$), allowing carriers to follow the AC signal and inject into the blue QLED, resulting in the capacitance rise. For example, under an applied voltage of 2.2 V, the device capacitance rises at 100 Hz but not at 500 Hz [Fig. 2(a)], indicating that the carrier can follow the AC signal at 100 Hz but finds it hard to do so at 500 Hz. Therefore, τ_{tr} can be estimated to be 2 ms $< \tau_{tr} <$ 10 ms. Using this method, τ_{tr} at other bias can be approximately calculated. At an applied voltage of 2.4 V, the capacitance rises at 1 kHz instead of 5 kHz, so τ_{tr} can be estimated to be 0.2 ms $< \tau_{tr} <$ 1 ms. At 2.7 V, where the capacitance rises at 5 kHz, τ_{tr} should be smaller than 0.2 ms.

To precisely assess τ_{tr} and τ_r, C–f measurements were carried out under an applied voltage ranging from 2.6 to 3.1 V. As shown in Fig. 3(a), the device capacitance is nearly contributed by C_g above 10 kHz, indicating negligible charge injection at higher frequencies. Upon decreasing the frequency, a clear peak emerges in the C–f characteristics, which implies the competition between the redistribution of an injected carrier and the recombination process.[7,10,19,23] Typically, charge accumulation or charge trapping of injected carriers leads to an increase in capacitance, while carrier recombination is the primary cause of capacitance drop. Therefore, before reaching the peak point, capacitance is primarily influenced by the redistribution of injected carriers, while charge recombination process dominates the capacitance change after the peak point. To better understand these carrier processes and their impact on device capacitance, it is essential to

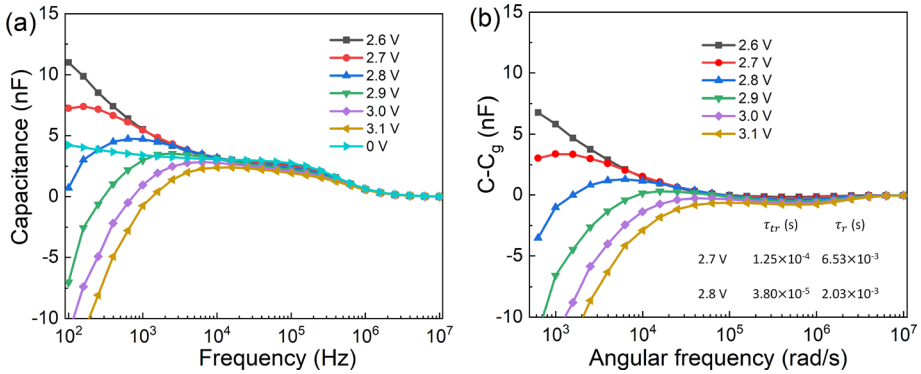

FIG. 3. (a) C–f and (b) (C–C_g)-ω characteristics of the blue QLED at varied applied frequencies.

quantitatively determine the characteristic times τ_{tr} and τ_r. These two parameters can be extracted using a simplified equation as follows:[7,25,26]

$$C(\omega) = C_g + \frac{\chi_1 C_g}{1+(\omega\tau_{tr})^2} - \frac{\chi_2 C_g}{1+(\omega\tau_r)^2}. \quad (1)$$

Here, ω is the angular frequency, χ_1 and χ_2 are dimensionless constants, and $C(\omega)$ is the device capacitance, which includes C_g, carrier injection-induced capacitance rise (the second item), and carrier recombination-induced capacitance drop (the third item). Although the fitting equation is simple, it can well describe the frequency-dependent complex capacitance by considering the underlying physical process. Figure 3(b) shows the additional capacitance (C–C_g) vs ω characteristics. At 2.6 V, C–C_g is continuously increasing as the frequency transitions from high to low, indicating that the additional capacitance is primarily contributed by a carrier injection-induced capacitance rise. Therefore, it is hard to obtain both τ_{tr} and τ_r through equation fitting. Similarly, the additional capacitance is mainly contributed by a carrier recombination-induced capacitance drop at the applied voltage of 2.9–3.1 V, so τ_{tr} and τ_r at these voltages are difficult to extract as well. At the working voltages of 2.7 and 2.8 V, there are both increased and decreased items in the device capacitance, so Eq. (1) can be effectively fitted at 2.7 and 2.8 V (Fig. S2). As illustrated in Fig. 3(b), the derived values for τ_{tr} are estimated to be 1.25×10^{-4} s and 3.80×10^{-5} s at 2.7 and 2.8 V, respectively. Correspondingly, the estimated values for τ_r are 6.53×10^{-3} s and 2.03×10^{-3} s at 2.7 and 2.8 V, respectively. Upon analyzing the fitting results, the frequency at which the capacitance rises at 2.7 V should be below 8 kHz, consistent with the C–V curve presented in Fig. 2(a). Notably, we did not observe the capacitance rise under 2.7 V in a C–V curve at 10 kHz (Fig. S3), in this case, τ_{tr} is larger than τ_{ac}, suggesting that carriers are unable to follow the AC signal, thereby validating our fitting results. Furthermore, it is worth mentioning that τ_r is one or two orders larger than τ_{tr}, indicating that the carrier recombination process dominates in a low frequency region, whereas the carrier injection process dominates in a higher frequency region, a phenomenon also reflected in Fig. 3.

Regarding the characteristic voltage V_p in the C–V curve, it comes after V_t. In QLED, charge injection occurs alongside charge recombination, and both carrier processes have an impact on the device capacitance. Before V_p, the charge injection rate is faster than the carrier recombination rate, resulting in a charge accumulation in blue QLED. Consequently, the device capacitance tends to increase. After V_p, the carrier recombination process dominates, consuming the free carrier, thereby leading to the capacitance drop. Therefore, carrier behavior reaches a quasi-equilibrium state at V_p, indicating a balanced process of charge injection and recombination,[23] it is determined by the interaction of τ_{tr} and τ_r. As depicted in Fig. S4, we have collected denser C–V and C–f curves. The red arrows represent the variation trend of V_t and V_p in C–V curves. V_t tends to rise as the frequency increases, it corresponds to the red arrows in a C–f curve, where the capacitance starts to rise. For example, V_t in a C–V curve of blue QLED at 100 Hz is 2.2 V. While in a C–f curve, the capacitance at 2.2 V starts to rise (compared to C_g) near 100 Hz, which corresponds to the V_t point. Likewise, the variation trend of V_p in C–V curves matches exactly with the voltages at peak capacitance for each frequency in the C–f curve. Moreover, we also observe the frequency-dependent characteristic voltages in the C–V curve of a red QLED, which is consistent with our findings in blue QLED. That is to say, the characteristic voltages in a C–V curve can be used to depict the carrier behavior in QLED in general, and it is determined by the characteristic times at the selected working voltage.

Apart from the analysis of characteristic voltages, the C–V curve is helpful to evaluate charge accumulation or charge leakage in a blue QLED. Figure 4 illustrates three distinct C–V curves at 1 kHz, which correspond to different carrier processes in blue QLED. Among them, Fig. 4(a) show a typical C–V curve of a control device with a structure of ITO/PEDOT:PSS/TFB/blue QD/ZnMgO/Al, it showcases the typical characteristic voltages. In Fig. 4(b), the control blue QLED is shelf-aged for a long time, which forms defects in the device (Fig. S5). It is clear that the capacitance starts to rise at 2.2 V and drops after 2.8 V. However, unlike the C–V curve of the control device, it resumes an increase at 4.1 V, indicating a charge accumulation process in the shelf-aged device. In Fig. S5, the Nyquist plot (at 4.1 V) of the shelf-aged device shows two semicircle characteristics, indicating an additional charge trapping process, which causes the capacitance to rise again. As a comparison, we did not observe any characteristic voltage in Fig. 4(c) with a NiO_x as the hole injection layer. This absence is attributed to the weaker hole injection using NiO_x nanoparticle, allowing electrons in the QD layer to leak into the HTL (Fig. S6). Consequently, it is difficult for carrier accumulation, and capacitance rise is absent. We have to notice that, unlike the C–V curve of the control device at 10 kHz (Fig. S3), there is no characteristic voltage because

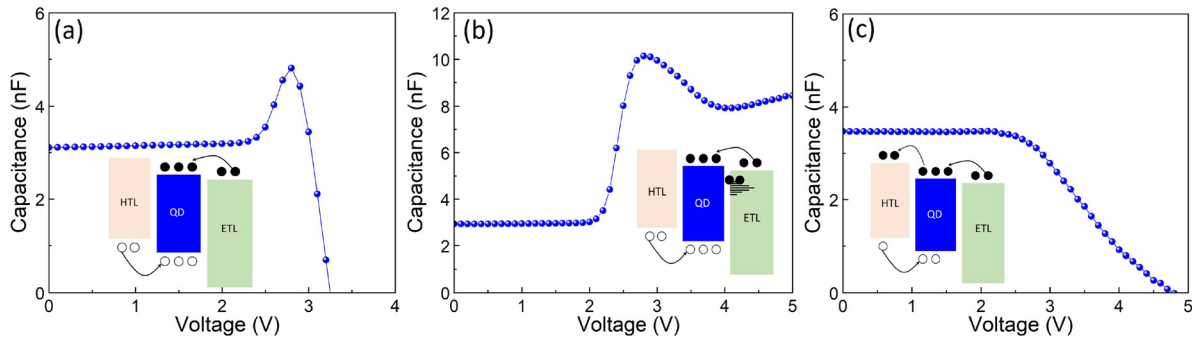

FIG. 4. C–V characteristics of (a) control blue QLED, (b) shelf-aged blue QLED, and (c) NiO_x-based blue QLED. The insets illustrate the corresponding carrier processes of (a) charge injection in control device, (b) charge accumulation, and (c) charge leakage.

$\tau_{tr} > \tau_{ac}$, i.e., the carrier cannot follow the AC signal at all. However, for NiO_x-based QLED, it is difficult to establish a space charge in the device owing to serious charge leakage.[27] Fortunately, when a self-assembled molecule (SAM) is linked to the surface of NiO_x nanoparticles, it significantly suppresses electron leakage (Fig. S6). As a result, we observe the evident characteristic voltages in the C–V curve of the SAM modified device; the device capacitance rises at 2.3 V and drops after 2.8 V (Fig. S7). It indicates that SAM modification improves the performance of the NiO_x-based QLED device. Therefore, the feature of the C–V curve aids in evaluating charge accumulation or leakage in the device, implying that the C–V characteristic is a sensitive probe to monitor the charge dynamics in a QLED.

In conclusion, the proposed C–V models in previous works are not appropriate to depict the carrier processes owing to the frequency-dependent characteristics of capacitance. Therefore, the charge injection and recombination points should be extracted from the J–V–L characteristic rather than a C–V curve. As for the characteristic voltage in a C–V curve, the transition voltage V_t corresponds to the point at which additional carriers, generated by the AC signal, are injected into the device, while V_p represents the quasi-equilibrium state of the carrier in the device, indicating a balanced process of charge injection and recombination. These characteristic voltages are determined by the voltage-dependent characteristic times. Finally, we illustrate distinct C–V characteristics that correspond to various carrier processes. These findings enhance our comprehension of carrier behavior in AC measurements and the charge dynamics of QLED.

See the supplementary material for details on the EL spectrum of blue QLED, fitting discrepancies of the *(C-Cg)-ω* characteristic of the original and fitting data, C–V characteristic of blue QLED at 10 kHz, denser C–V and C–f curves of blue QLED, Nyquist plots of the control device and shelf-aged device, and the J–V and C–V characteristics of blue QLEDs with NiO_x or NiO_x/SAM HIL.

This work was supported by the National Key Research and Development Program of China (Nos. 2022YFB3602903, 2021YFB3602703, and 2022YFB3606504), the National Natural Science Foundation of China (No. 62122034), the Guangdong University Key Laboratory for Advanced Quantum Dot Displays and Lighting (No. 2017KSYS007), the Shenzhen Key Laboratory for Advanced Quantum Dot Displays and Lighting (No. ZDSYS201707281632549), the Shenzhen Science and Technology Program (No. JCYJ20220818100411025), and the Shenzhen Development and Reform Commission Project (Grant No. XMHT20220114005).

AUTHOR DECLARATIONS

Conflict of Interest

The authors have no conflicts to disclose.

Author Contributions

Xiangwei Qu: Conceptualization (equal); Data curation (equal); Formal analysis (equal); Investigation (equal); Methodology (equal); Writing – original draft (equal). **Jingrui Ma:** Investigation (equal); Methodology (equal). **Kai Wang:** Methodology (equal). **Xiao Wei Sun:** Conceptualization (equal); Funding acquisition (equal); Project administration (equal); Resources (equal); Supervision (equal); Writing – review & editing (equal).

DATA AVAILABILITY

The data that support the findings of this study are available from the corresponding author upon reasonable request.

REFERENCES

[1]X. Dai, Z. Zhang, Y. Jin, Y. Niu, H. Cao, X. Liang, L. Chen, J. Wang, and X. Peng, Nature **515**(7525), 96–99 (2014).
[2]L. Qian, Y. Zheng, J. Xue, and P. H. Holloway, Nat. Photonics **5**(9), 543–548 (2011).
[3]X. Dai, Y. Deng, X. Peng, and Y. Jin, Adv. Mater. **29**(14), 1607022 (2017).
[4]B. S. Mashford, M. Stevenson, Z. Popovic, C. Hamilton, Z. Zhou, C. Breen, J. Steckel, V. Bulovic, M. Bawendi, S. Coe-Sullivan, and P. T. Kazlas, Nat. Photonics **7**(5), 407–412 (2013).
[5]Y. Deng, F. Peng, Y. Lu, X. Zhu, W. Jin, J. Qiu, J. Dong, Y. Hao, D. Di, Y. Gao, T. Sun, M. Zhang, F. Liu, L. Wang, L. Ying, F. Huang, and Y. Jin, Nat. Photonics **16**(7), 505–511 (2022).
[6]Y. Shirasaki, G. J. Supran, M. G. Bawendi, and V. Bulović, Nat. Photonics **7**(1), 13–23 (2013).
[7]L. Zhang, H. Nakanotani, and C. Adachi, Appl. Phys. Lett. **103**(9), 093301 (2013).
[8]V. Shrotriya and Y. Yang, J. Appl. Phys. **97**(5), 054504 (2005).
[9]S. Nowy, W. Ren, A. Elschner, W. Lövenich, and W. Brütting, J. Appl. Phys. **107**(5), 054501 (2010).
[10]C. Blauth, P. Mulvaney, and T. Hirai, J. Appl. Phys. **125**(19), 195501 (2019).
[11]X. Xiao, T. Ye, J. Sun, X. Qu, Z. Ren, D. Wu, S. Ding, X. W. Sun, W. C. H. Choy, and K. Wang, Appl. Phys. Lett. **120**(24), 243501 (2022).
[12]X. Qu and X. Sun, J. Semicond. **44**(9), 091603 (2023).
[13]Y. Fang, P. Bai, J. Li, B. Xiao, Y. Wang, and Y. Wang, ACS Appl. Mater. Interfaces **14**(18), 21263–21269 (2022).
[14]P. Tang, L. Xie, X. Xiong, C. Wei, W. Zhao, M. Chen, J. Zhuang, W. Su, and Z. Cui, ACS Appl. Mater. Interfaces **12**(11), 13087–13095 (2020).
[15]T. Kim, K. H. Kim, S. Kim, S. M. Choi, H. Jang, H. K. Seo, H. Lee, D. Y. Chung, and E. Jang, Nature **586**(7829), 385–389 (2020).
[16]X. Qu, G. Xiang, J. Ma, P. Liu, A. K. K. Kyaw, K. Wang, and X. W. Sun, Appl. Phys. Lett. **122**(11), 113501 (2023).
[17]M. Zhang, F. Guo, Q. Zhou, T. Zhong, B. Xiao, L. Zou, Q. You, B. You, Y. Li, X. Liu, H. Liu, J. Yan, and J. Liu, J. Lumin. **234**, 117946 (2021).
[18]M. Zhang, F. Guo, S. Lei, T. Zhong, B. Xiao, C. Liu, L. Wang, J. Chen, Q. You, J. Liu, and R. Yang, Dyes Pigm. **195**, 109703 (2021).
[19]X. Qu, J. Ma, C. Shan, P. Liu, A. K. K. Kyaw, and X. W. Sun, Appl. Phys. Lett. **121**(11), 113507 (2022).
[20]S. He, X. Tang, Y. Deng, N. Yin, W. Jin, X. Lu, D. Chen, C. Wang, T. Sun, Q. Chen, and Y. Jin, Nat. Commun. **14**(1), 7785 (2023).
[21]Y. Sun, W. Chen, Y. Wu, Z. He, S. Zhang, and S. Chen, Nanoscale **11**(3), 1021–1028 (2019).
[22]H. Zhang and S. Chen, J. Mater. Chem. C **7**(8), 2291–2298 (2019).
[23]J. Ma, H. Tang, X. Qu, G. Xiang, S. Jia, P. Liu, K. Wang, and X. W. Sun, Chin. Phys. Lett. **39**(12), 128401 (2022).
[24]Z. Wu, P. Liu, X. Qu, J. Ma, W. Liu, B. Xu, K. Wang, and X. W. Sun, Adv. Opt. Mater. **9**(17), 2100389 (2021).
[25]S. Berleb and W. Brutting, Phys. Rev. Lett. **89**(28), 286601 (2002).
[26]E. Ehrenfreund, C. Lungenschmied, G. Dennler, H. Neugebauer, and N. S. Sariciftci, Appl. Phys. Lett. **91**(1), 012112 (2007).
[27]W. Ji, S. Liu, H. Zhang, R. Wang, W. Xie, and H. Zhang, ACS Photonics **4**(5), 1271–1278 (2017).

Supplementary Material

Characteristic voltages and times from capacitance-voltage analysis of quantum dot light-emitting diodes

Xiangwei Qu[1,2], Jingrui Ma[1,2], Kai Wang[1,2], and Xiao Wei Sun[1,2]

1 Institute of Nanoscience and Applications, Southern University of Science and Technology, Shenzhen 518055, China.

2 Key Laboratory of Energy Conversion and Storage Technologies (Southern University of Science and Technology), Ministry of Education, Guangdong University Key Laboratory for Advanced Quantum Dot Displays and Lighting, Shenzhen Key Laboratory for Advanced Quantum Dot Displays and Lighting, and Department of Electrical and Electronic Engineering, Southern University of Science and Technology, Shenzhen 518055, China

E-mail: sunxw@sustech.edu.cn

Supplementary material include: EL spectrum of blue QLED, fitting discrepancies of *(C-Cg)-ω* characteristic of original and fitting data, C-V characteristic of blue QLED at 10 kHz, denser C-V and C-f curves of blue QLED. Nyquist plots of control device and shelf aged device, J-V and C-V characteristic of blue QLEDs with NiOx or NiOx/SAM HIL.

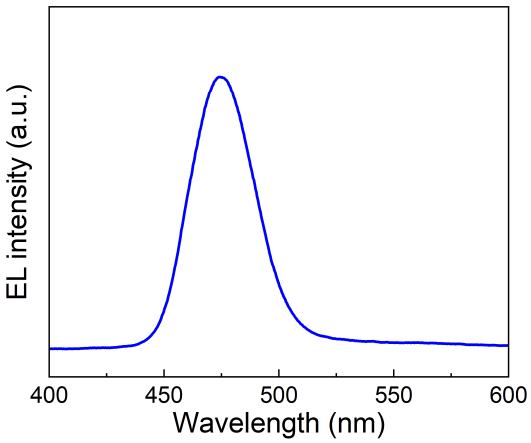

Fig. **S**1 EL spectrum of blue QLED.

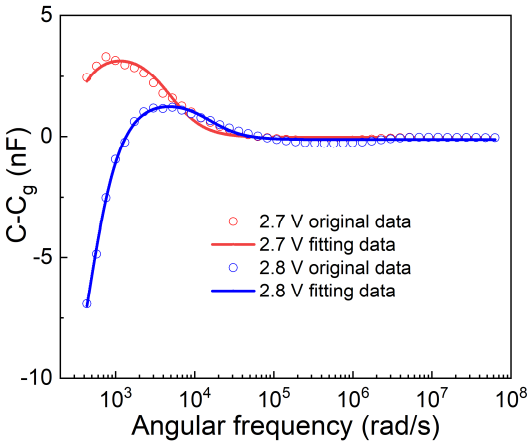

Fig. **S**2 Original and fitting *(C-Cg)-ω* curves of blue QLED at 2.7 and 2.8 V.

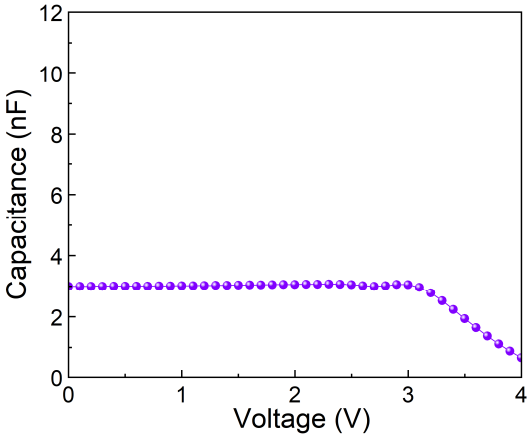

Fig. **S**3 C-V characteristic of blue QLED at 10 kHz.

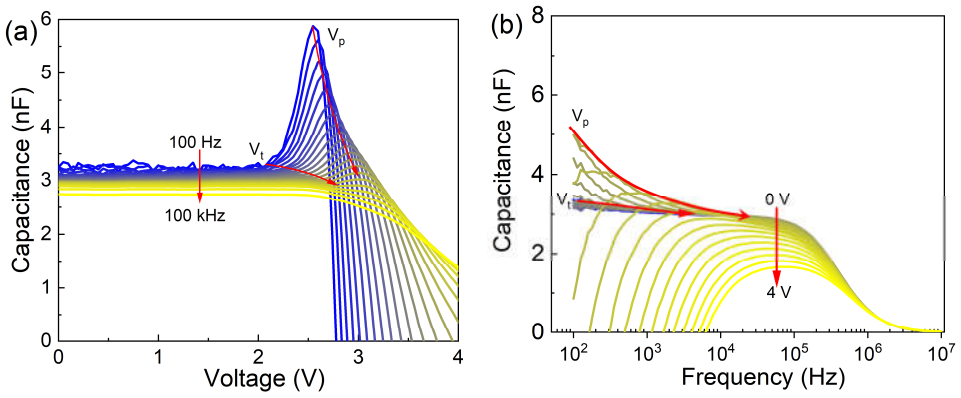

Fig. **S**4 C-V and C-f characteristics of blue QLEDs.

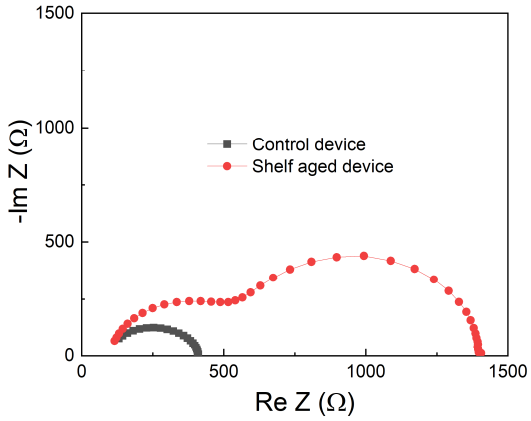

Fig. **S**5 Nyquist plots of control device and shelf aged device at 4.1 V.

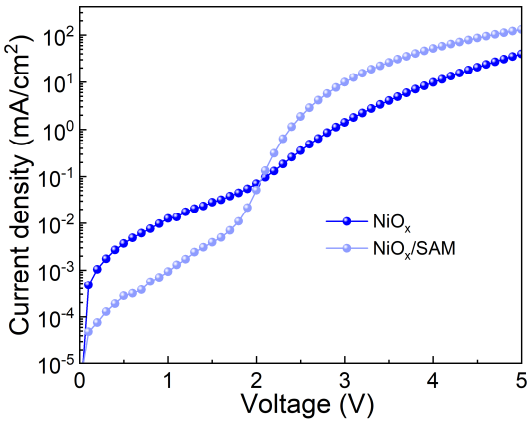

Fig. **S**6 J-V characteristics of blue QLEDs with NiO_x or NiO_x/SAM HIL.

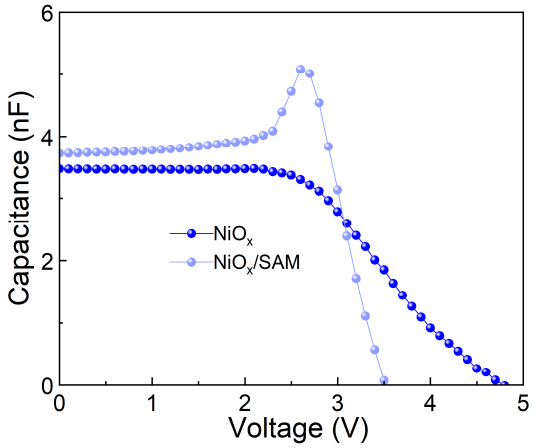

Fig. **S**7 C-V characteristics of blue QLEDs with NiO_x or NiO_x/SAM HIL.